Supplementary Information

Non-associative phase separation in an evaporating droplet as a model for prebiotic compartmentalization

Wei Guo,[†,⁋] Andrew Kinghorn,[‡,⁋] Yage Zhang,[†] Qingchuan Li,[†] Aditi Dey Poonam,[†] Julian A. Tanner,[‡,*] Ho Cheung Shum[†,*]

† Department of Mechanical Engineering, Faculty of Engineering, The University of Hong Kong, Hong Kong (SAR), China

‡ School of Biomedical Sciences, LKS Faculty of Medicine, The University of Hong Kong, Hong Kong (SAR), China

⁋ These authors contributed equally to this work.

* To whom correspondence should be addressed:

Email: jatanner@hku.hk

ashum@hku.hk

Content

1. Supplementary text
2. Table S1
3. Figures S1 to S12
4. Captions for Movies S1 to S6
5. SI References
6. Movies S1 to S6

Supplementary Information Text

S1. Materials

The ribozyme sequences and Broccoli DNA template were purchased from Integrated DNA Technology (IDT).

Hammerhead Ribozyme DNA template
TTAGGCGCGTTTCGTCCTATTTGGGACTCATCAGCTGGATCCTATAGTGAGTC
GTATTATATTGAACAAGCTC

Hammerhead Substrate
/56-TAMN/rCrGrUrGrCrGrUrCrCrUrGrGrArU/36-FAM/

X-Motif Ribozyme DNA template
GTCCTGTCGCTTGGCTCTCTTCCTTGGCTCTCCCTATAGTGAGTCGTATTATAT
TGAACAAGCTCGTAT

X-Motif Substrate
/5ATTO488N/rArGrUrCrCrUrGrArUrGrGrUrUrArCrUrCrCrArArU/3BHQ_1/

S2. Evaporation flux calculation

For a sessile droplet with a shape of a spherical cap, the droplet height h is a function of droplet contact angle θ and droplet radius R, and can be written as

$$h(r,t)=\sqrt{\frac{R^2}{\sin^2\theta}-r^2}-R\cot\theta$$

The droplet evaporation rate can therefore be calculated as

$$\frac{dM}{dt}=-\int_0^R J(r)\sqrt{1+(\partial_r h)^2}\,2\pi dr$$

where $J(r)$ is evaporation flux that is modeled by the vapor diffusion equation $\nabla^2 n=0$. Here the boundary conditions of the diffusion process are set as: $n=n_\infty$ far away from the droplet and $n=n_s$ at the liquid-air interface. Here n_s and n_∞ are the saturated vapor concentration and ambient vapor concertation (decided by humidity $n_\infty=RH\cdot n_s$), respectively. Then the evaporation flux can be written as $J(r)=-D\nabla n$, where D is vapor diffusion coefficient. As a result, the droplet evaporation rate has the analytical solution of

$$\frac{dM}{dt}=-\pi RD(n_s-n_\infty)\left[\frac{\sin\theta}{1+\cos\theta}+4\int_0^\infty \frac{1+\cosh 2\theta\tau}{\sinh 2\pi\tau}\tanh[(\pi-\theta)\tau]d\tau\right]$$

In our experiments, a sessile droplet of $0.5\mu L$ pipetted on the glass slide has an initial radius of $R_0\approx 1mm$ and the initial contact angle of $\theta\approx 40°$. Substituting $n_s=17.3g/m^3$, and $RH\approx 60\%$ into the equation, we have $dM/dt\approx 0.9$ μg/s. This result can be further confirmed based on the evaporation time of a $0.5\mu L$ droplet (with water mass of about $425\mu g$), which is estimated to be about 400 seconds, with an average evaporation rate of $1.06\mu g/s$, consistent with the calculated value from the model. Figure ***S5*** shows the calculated local droplet evaporation rate as a function of R_i based on this model, where the local evaporation rate has a magnitude of

$$\frac{dM_i}{dt}=-\int_0^{R_i} J(r)\sqrt{1+(\partial_r h)^2}\,2\pi dr$$

This suggests that the local evaporation rate along droplet surface is highly non-uniform.

Here we choose a calculation domain with a spanwise of $0.05R_0$ from the edge of the droplet. The volume of the calculation domain, the initial mass of solutions in the calculation domain, and the mass change rate due to evaporation are, respectively,

$$V_0=\int_{0.95R}^R h(r.t)\,2\pi r dr$$

$$M_0=\rho V_0$$

$$\frac{dM_0}{dt}=-\int_{0.95R}^R J(r)\sqrt{1+(\partial_r h)^2}\,2\pi dr$$

As a result, the polymer concentration after the evaporation time of Δt is

$$c'=M_0c_0/\left(M_0+\frac{dM_0}{dt}\cdot\Delta t\right)$$

where c_0 is the initial polymer concentration. The calculation results for droplets in the two different experiments are listed below in **Table S1**.

$\boldsymbol{c_0}$	$\boldsymbol{V_0}$	$\boldsymbol{M_0}$	$\boldsymbol{dM_0/dt}$	$\boldsymbol{c'}$ **(after** $\boldsymbol{\Delta t = 5\ s}$**)**
PEG: 5wt% Dextran: 10wt%	$5.48\ nL$	$5.72\ \mu g$	$-0.194\ \mu g/s$	PEG: 6.02wt% Dextran: 12.04wt%
PEG: 9wt% Dextran: 4wt%		$5.63\ \mu g$		PEG: 10.88wt% Dextran: 4.84wt%

Table S1. Parameters in the calculation domain. A spanwise of $0.05R_0$ from the edge of the droplet is selected. c_0 is the initial polymer concentration in the domain. V_0 and M_0 are the volume of the domain and the mass of solution inside the domain, respectively. dM_0/dt is the rate of mass change due to evaporation. c' is the polymer concentration after 5 seconds of evaporation.

S3. Marangoni stress calculation

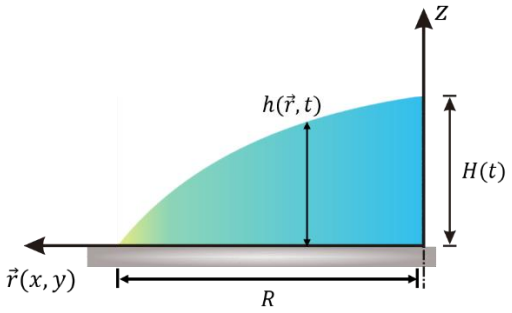

In our model system, the aspect ratio of droplet is $H/R \approx 0.18$. The lubrication approximation can be applied to calculate the flow velocity $\vec{u}$ and volume flux $\vec{Q}$. Here $\vec{Q}$ is defined as

$$\vec{Q}(\vec{r},t) = \int_0^{h(\vec{r},t)} \vec{u}(\vec{r},z,t)dz$$

With the lubrication approximation, $\vec{u}$ and $\vec{Q}$ can be obtained using the following equations:

$$\vec{u}(\vec{r},z,t) = \frac{1}{\mu}\frac{\partial p}{\partial r}\left(\frac{1}{2}z^2 - h(\vec{r},t)z\right) + \frac{z}{\mu}\frac{\partial \gamma}{\partial r}$$

$$\vec{Q}(\vec{r},t) = \frac{h^3}{3\mu}\nabla(\gamma\nabla^2 h) + \frac{h^2}{2\mu}\nabla\gamma$$

where μ is the viscosity, γ is the surface tension, and p is the capillary pressure ($p = -\gamma\nabla^2\tilde{h}$), respectively.

The first term of $\vec{Q}(\vec{r},t)$ indicates the capillary flow induced by the gradient of Laplace pressure. The second term denotes the Marangoni flow driven by the Marangoni effects. Therefore, for sufficiently small $\Delta\gamma$ or $\Delta\gamma/\gamma$, the magnitude of capillary flow and Marangoni flow can be estimated as

$$Q_{Ca} \sim \frac{\gamma H^4}{\mu R^3},\ Q_{Ma} \sim \frac{\Delta\gamma}{\mu}\frac{H^2}{R}$$

The ratio of these two terms is estimated as

$$\frac{Q_{Ma}}{Q_{Ca}} \sim \frac{R^2\Delta\gamma}{H^2\gamma}$$

Substituting the experimental parameters: $H \approx 170\mu m$, $R \approx 0.96mm$, $\gamma \approx 63.5mN/m$, and then $\Delta\gamma$ that satisfies $Q_{Ma}/Q_{Ca} = 1$ is calculated to be $\Delta\gamma \approx 2mN/m$

This indicates that with small H/R, a small Marangoni force is sufficient to suppress the outward capillary flow. In our model system, a surface tension difference of $2mN/m$ along the droplet surface can be easily achieved due to non-uniform evaporation rate. For example, for droplets composed of 5 wt% PEG and 10 wt% dextran, the initial surface tension is measured to be 63.5 mN/m. After a few seconds of evaporation, the composition

near the droplet edge is expected to be close to that in the top PEG-rich phase of the mixture containing 30 wt% PEG and 1 wt% dextran, with a surface tension of about 60 mN/m. This results in a surface tension difference of 3.5 mN/m.

Figure S1-S12

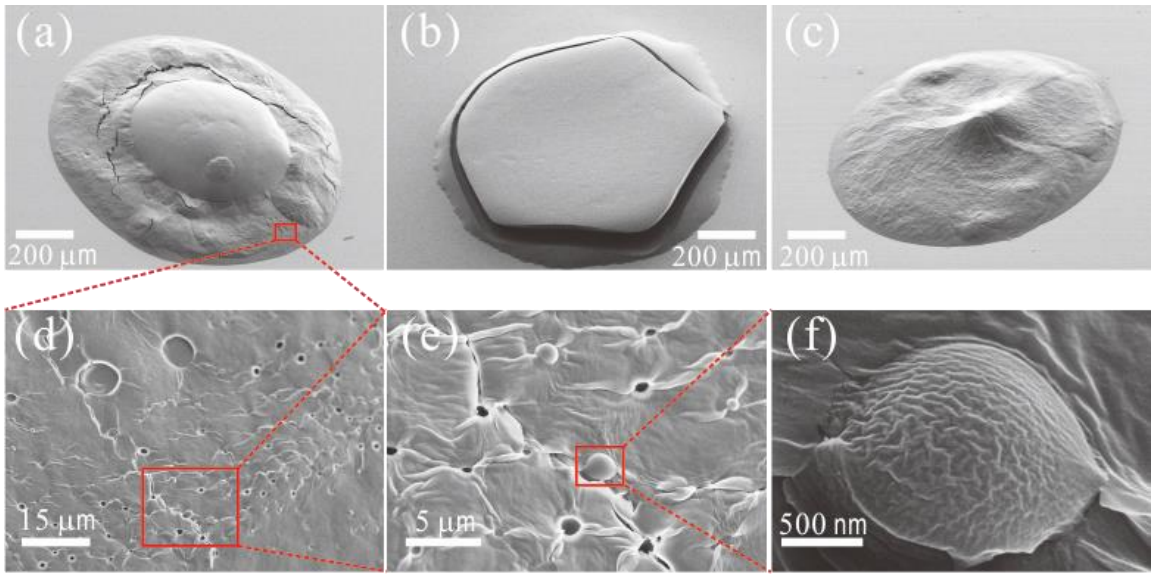

Fig. S1. (a), (b) and (c) show the deposition of a sessile droplet composed of 5wt% PEG and 10wt% dextran mixture, 10 wt% dextran solution, as well as the 10 wt% PEG solution, respectively. We can see that the surface morphology of PEG solution (Figure S1(c)) droplet deposited has much more stripes than that of dextran droplet deposited (Figure S1(b)), which looks much smoother. (d-f) Nano-scaled compartments in the deposited droplets.

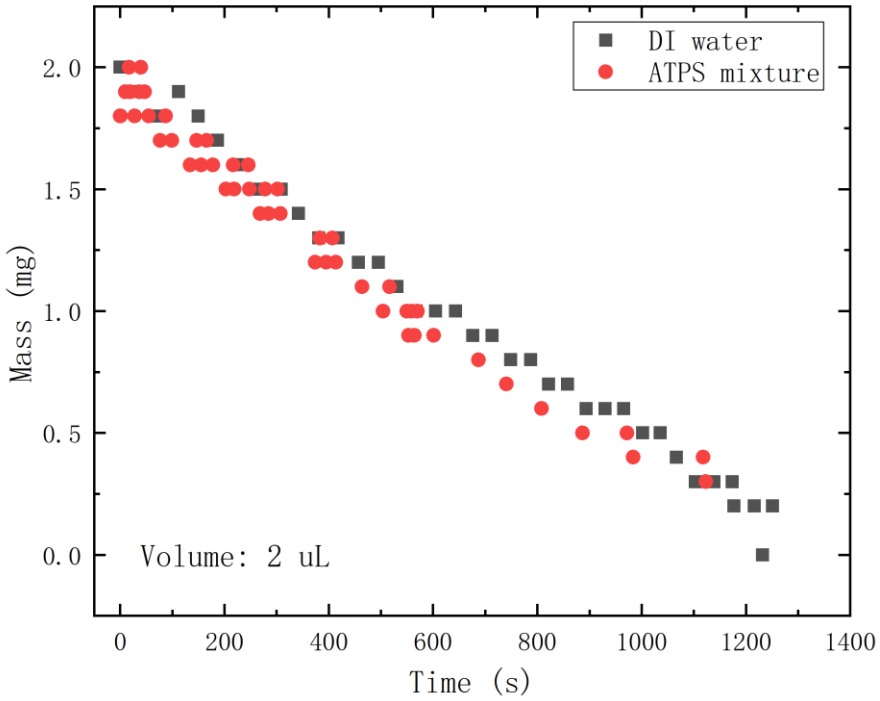

Fig. S2. Measured droplet mass as a function of evaporation time. A droplet with a volume of 2 uL was pipetted onto the glass. The mass of the droplet was recorded by an analytical balance. Both droplets of DI water and ATPS mixture show a linearly decreasing mass during evaporation.

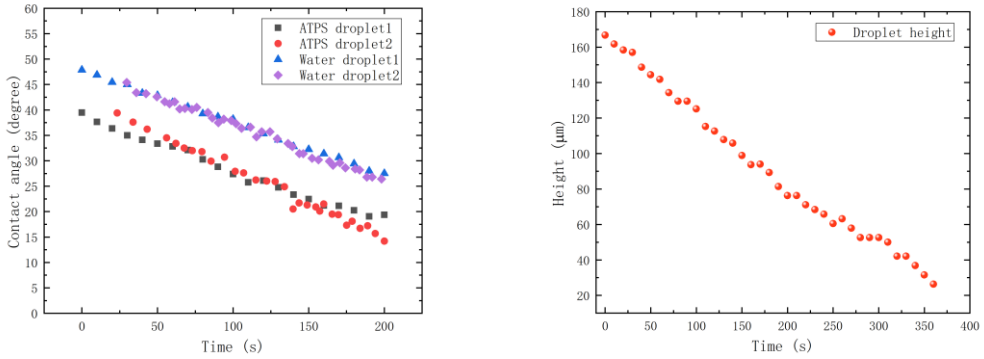

Fig. S3. Geometrical parameters of droplet during evaporation. (a) The decreasing contact angle of the sessile droplet during evaporation. The change of contact angle of the ATPS droplet is consistent with that of pure water droplet, except for their initial values. (b) Droplet height of an ATPS droplet as a function of evaporation time.

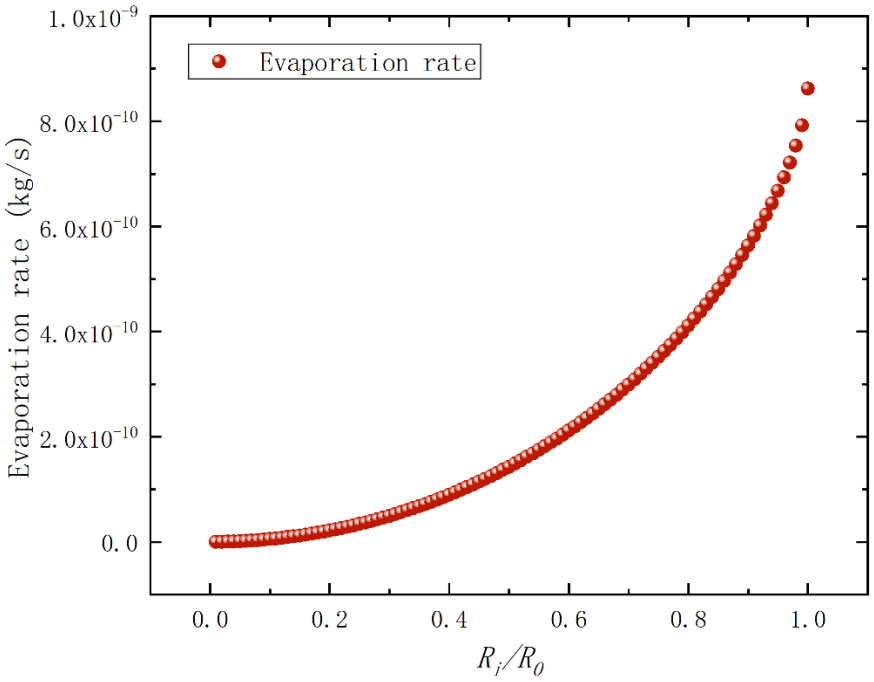

Fig. S4. Evaporation rate from the center of the sessile droplet ($R_i = 0$) to the edge of the sessile droplet ($R_i = R_0$). The non-uniform evaporation flux along the droplet surface determines the local evaporation rate.

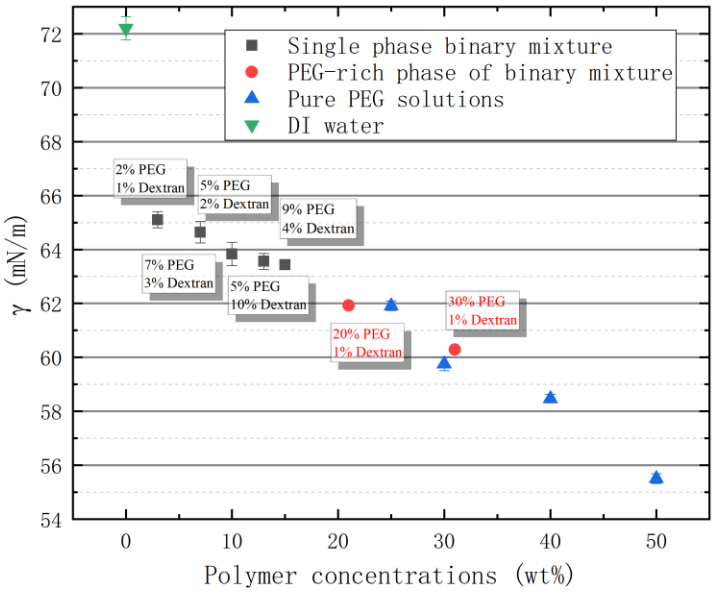

Fig. S5. A plot of the measured surface tension of the air-liquid interfaces as a function of polymer concentrations. The liquids tested include pure water, single-phase ATPS mixture, PEG solution, as well as phase-separated PEG-rich component. The surface tension was measured using the pendant droplet method[1] [2], with a custom MATLAB code

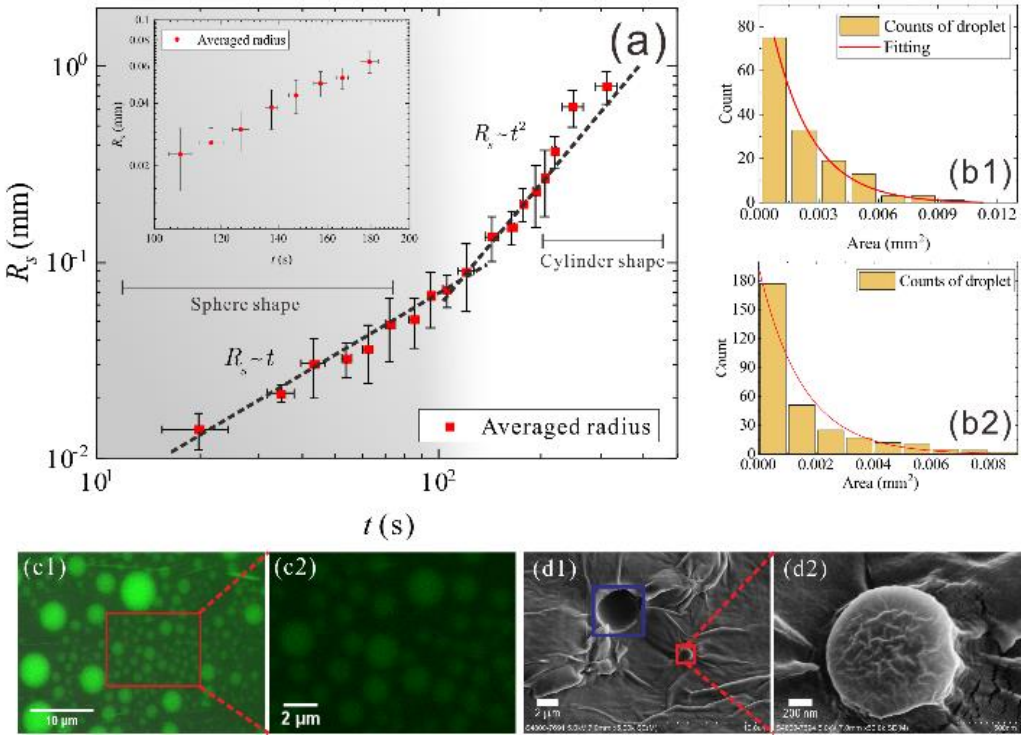

Fig. S6. (a) Time evolution of the average radius of dextran-rich droplets formed by LLPS in regime 2; Insert: Average radius evolution of PEG-rich droplets dispersed in the dextran-rich compartments in regime 1. The size of phase-separated compartments follows the scaling law of $R_s \sim t$ at the early evaporation stage ($t \leq 100s$). This is consistent with the Siggia's coarsening mechanism, where the hydrodynamic flow is the main transport process.[3] A transition from $R_s \sim t$ to $R_s \sim t^2$ at around 100s is observed, mainly due to the evaporation-driven decrease of sessile droplet height, resulting in a change in the shape of phase-separated droplets from spherical to cylindrical, and a corresponding increase in the droplet radius. (b) Size distribution of the phase-separated droplets in regime 1 (b1) and regime 2 (b2). The size distribution of these small droplets follows an exponential decay distribution (c1, c2) Confocal microscope images of nucleated dextran-rich compartments inside the sessile droplet; (d1, d2) SEM images showing dehydrated nano-scale compartments in the deposited sessile droplet.

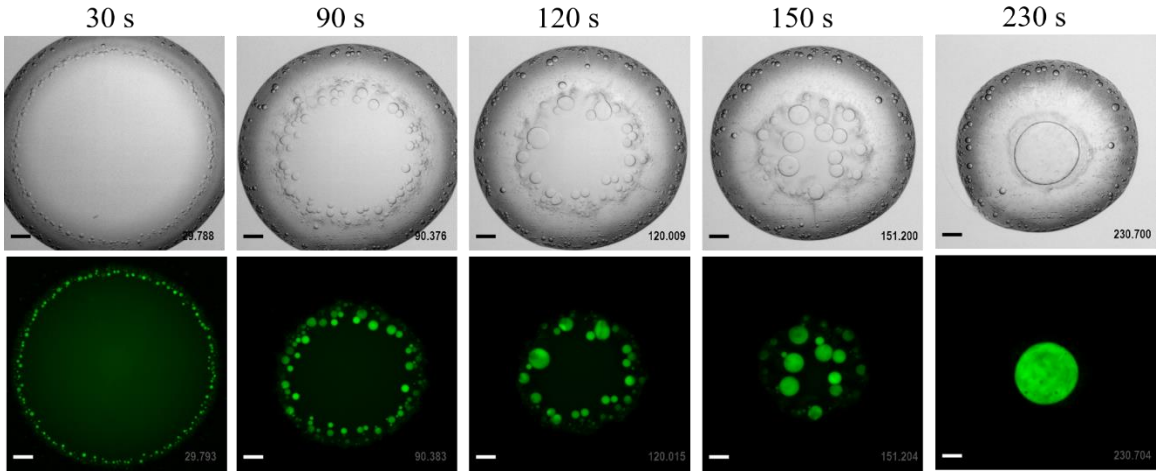

Fig. S7. Localization of fluorogenic RNA aptamer inside the evaporating sessile droplet. Sequences of fluorescence images (upper panel) and of bright field images (lower panel) suggest that RNA is localized into dextran-rich compartments during the LLPS process. The scale bar is 200 μm.

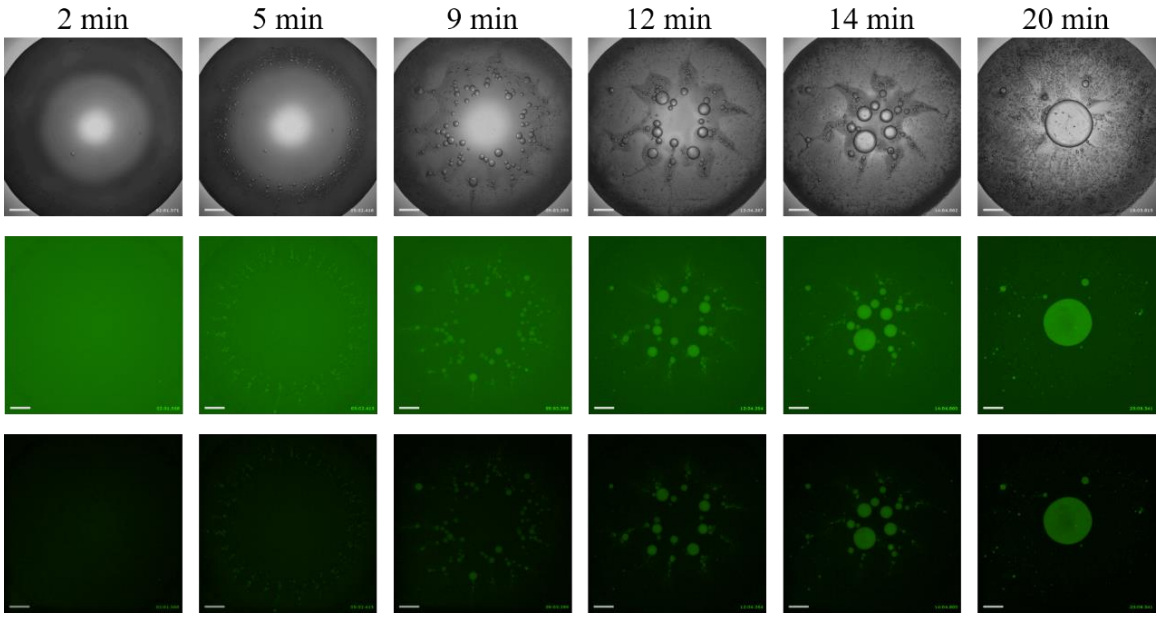

Fig. S8. Image sequence of hammerhead ribozyme cleavage inside the evaporating ATPS droplet. The upper panel, middle panel and lower panel represent the bright-field, fluorescence and background subtraction image sequence, respectively. The scale bar is 500 μm.

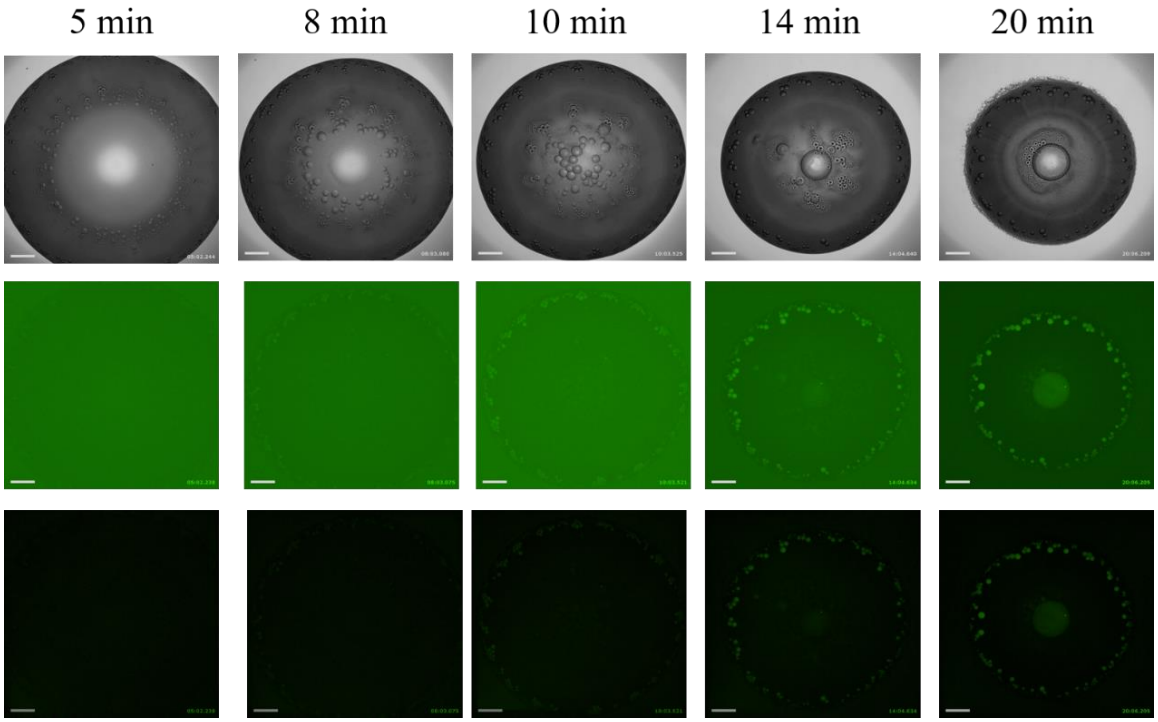

Fig. S9. Image sequence of control reaction inside the evaporating ATPS droplet, where only fluorophore-labelled substrate ithout any enzyme strand is present. The upper panel, middle panel and lower panel represent the bright-field, fluorescence and background subtraction image sequence, respectively. The scale bar is 500 μm.

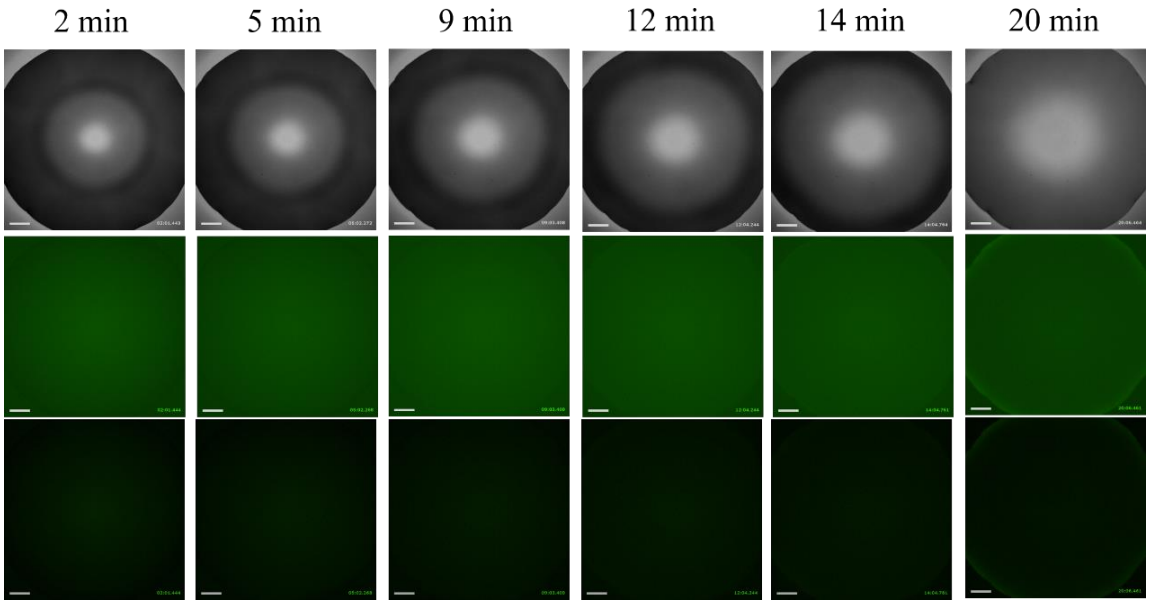

Fig. S10. Image sequence of control reaction inside the evaporating water droplet, where both fluorophore labelled substrate and enzyme strand have been added. The upper panel, middle panel and lower panel represent the bright-field, fluorescence and background subtraction image sequence, respectively. There is a slight fluorescent "coffee-ring"-like area formed at the edge after evaporation of 20 minutes. The fluorescence level is even lower than that in the ATPS control group (Figure S9). Hence, the cleavage reaction is largely restricted in the sessile droplet of pure water. We attribute the formation of the fluorescent area to the accumulation of fluorophore labelled substrate at the edge due to the outward capillary flow. The scale bar is 500 μm.

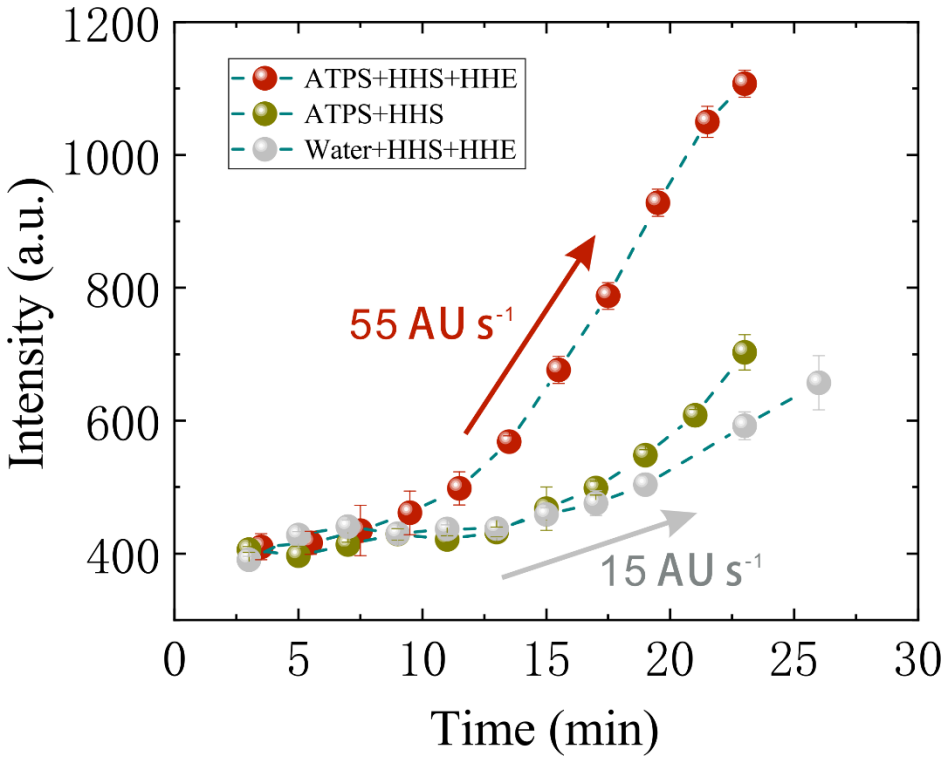

Fig. S11. Fluorescence intensity inside the sessile droplet as a function of time. Ribozyme activity in the dextran-rich compartments was enhanced more than 3-fold, in comparison to that in the water droplet.

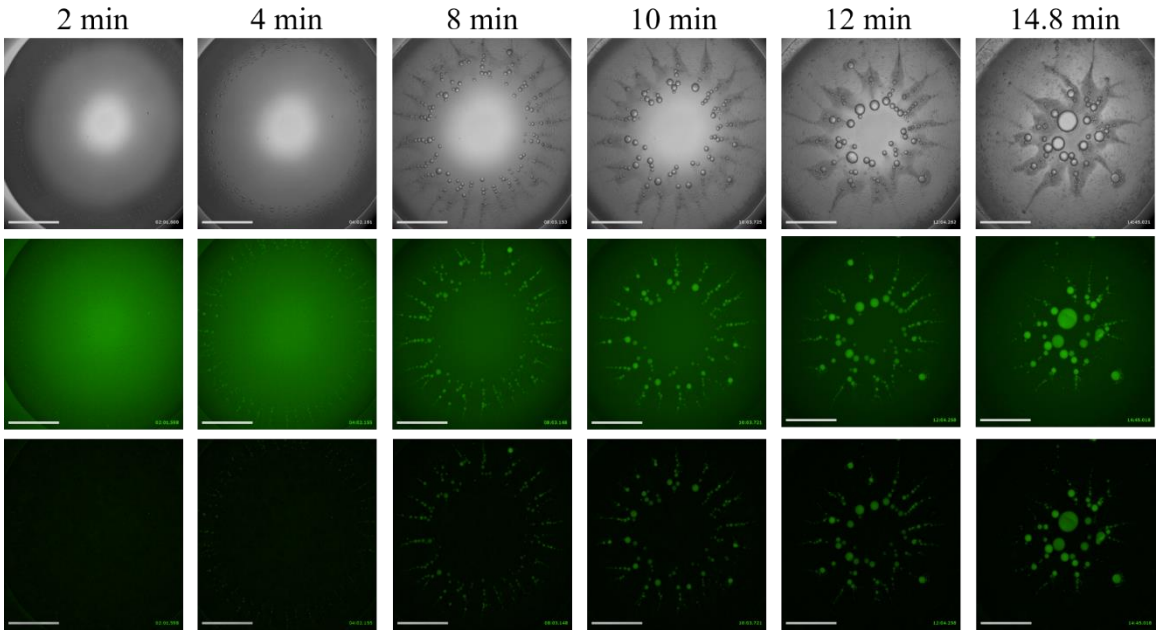

Fig. S12. Image sequence of X-motif ribozyme cleavage inside the evaporating ATPS droplet. The upper panel, middle panel and lower panel represent the bright-field, fluorescence and background subtraction image sequence, respectively. The scale bar is 1 mm.

Movie S1. Non-associative phase separation inside an evaporating ATPS droplet in Regime 1. For fluorescence imaging, 0.01 mg/mL fluorescein isothiocyanate−dextran (FITC-dextran, 500 kg/mol, Sigma-Aldrich) and 1 mg/mL Rhodamine B (>=95% (HPLC), Sigma-Aldrich) were added into the mixture.

Movie S2. Non-associative phase separation inside an evaporating ATPS droplet in Regime 2. For fluorescence imaging, 0.01 mg/mL fluorescein isothiocyanate−dextran (FITC-dextran, 500 kg/mol, Sigma-Aldrich) and 1 mg/mL Rhodamine B (>=95% (HPLC), Sigma-Aldrich) were added into the mixture.

Movie S3. DNA localization and compartmentalization inside an evaporating ATPS droplet. DNA was labeled with Cy5 dye (red fluorescence) and dextran is labeled with FITC.

Movie S4. RNA (aptamer) localization and compartmentalization inside an evaporating ATPS droplet. Broccoli RNA aptamer and DFHBI fluorophore were introduced into the mixture for fluorescence imaging.

Movie S5. *In-vitro* transcription **(**IVT) inside an evaporating ATPS droplet. Broccoli DNA aptamer and DFHBI fluorophore were introduced into the mixture for fluorescence imaging.

Movie S6. Hammerhead ribozyme cleavage inside an evaporating ATPS droplet.

SI References

[1] B. Song, J. Springer, Journal of Colloid and Interface Science, 184, 64-76 (1996).
[2] B. Song, J. Springer, Journal of Colloid and Interface Science 184, 77-91 (1996).
[3] E. D. Siggia, Physical Review A, 20, 595-605 (1979).
[4] G. S. Filonov, J. D. Moon, N. Svensen, S. R. Jaffrey, J Am Chem Soc, 136, 16299-16308 (2014).